For further investigation and verification, we measured the XPM in a single EAM by cutting it from the integrated device.

5.5.4 XPM

The same pump and probe lights are used as shown in Fig.5.11. Fig.5.14 shows the results of the Fabry-Perot measurement. While we increase the power of the pump light, the peak of the probe light shifts to the short wavelength, which implies the decrease of the phase and refractive index, as shown in Fig.5.15. From these two figures, apparent XPM is confirmed. This means the EAM works well as the phase modulator in the all-optical switch.

The insertion loss of the device is about 47dB, including 9dB/facet coupling loss between the fiber and device, at least 3*3dB loss caused by 3 cascaded MMIs, and 20 dB propagation loss as mentioned above. Due to the large insertion loss, the output is always smaller than –30dBm, which cannot be amplified effectively by EDFA. So no clear eye diagram is observed. In order to reduce the insertion loss, several methods can be applied. The most common one is to use AR coating. It can reduce the coupling loss down to 3 dB/facet. The second choice is to reduce the roughness of the sidewall by optimizing the dry etching conditions while forming high mesa. The third choice is to use ridge structure instead of high mesa. According to our experiments, the typical insertion loss of ridge structure with InGaAsP core is around 20dB/cm, much smaller than that of high mesa structure whose typical value is over 40dB/cm at 1500nm.

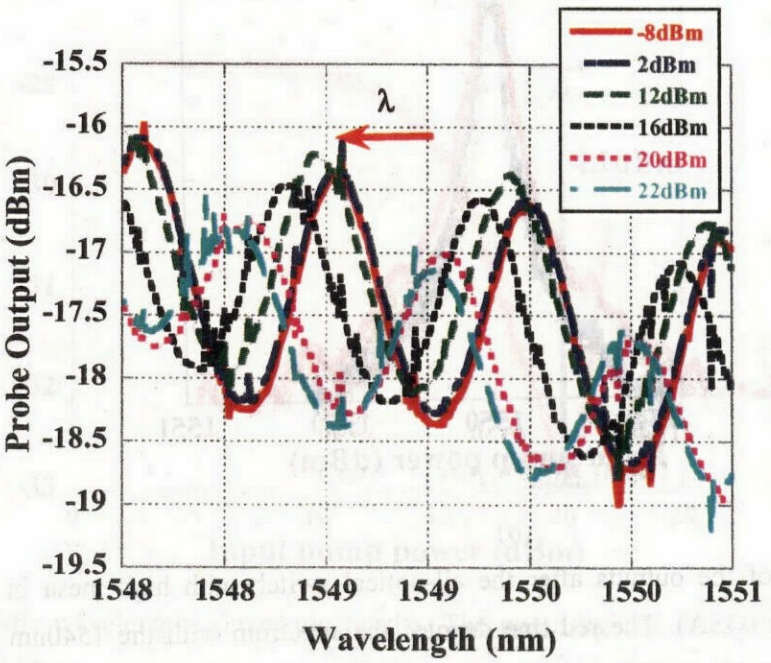

Fig.5.14 Fabry-Perot measurement for XPM of the EAM with high mesa waveguide..

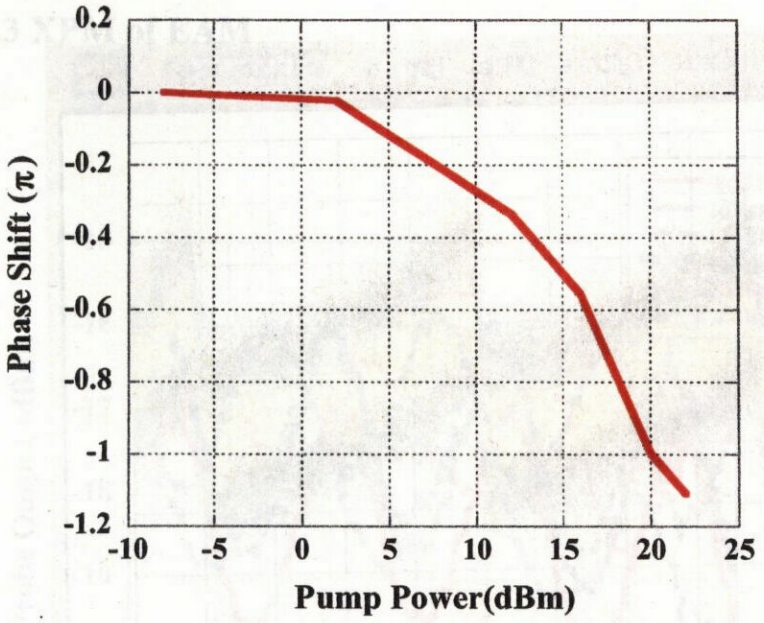

Fig.5.15 Phase shift of the EAM due to XPM.

5.6 Characterization of all-optical switch with ridge structure

Firstly, the coupling efficiency of the butt joint between the active and passive waveguides is investigated. This is done by the measurement of loss of the waveguide-EAM module, as shown in section 5.5. Then we demonstrated the dynamic operation of the wavelength conversion. For the results were not good, we investigated the performance of the EAM and MMI to find out the way for optimization.

5.6.1 Dynamic all optical switching

The experimental setup is almost the same with Fig.5.11. The difference is that here, we use 2.5Gb/s modulated signal.

Fig.5.16 shows the waveform of the modulated signal by 2.5Gb/s control pulse after the switch. We see that in this figure, the wavelength conversion is observed though the converted

signal is of very poor quality and the extinction ratio is quite small. The long tail is due to the long recovery in EAM without bias. This result confirms the availability of the novel all-optical switch.

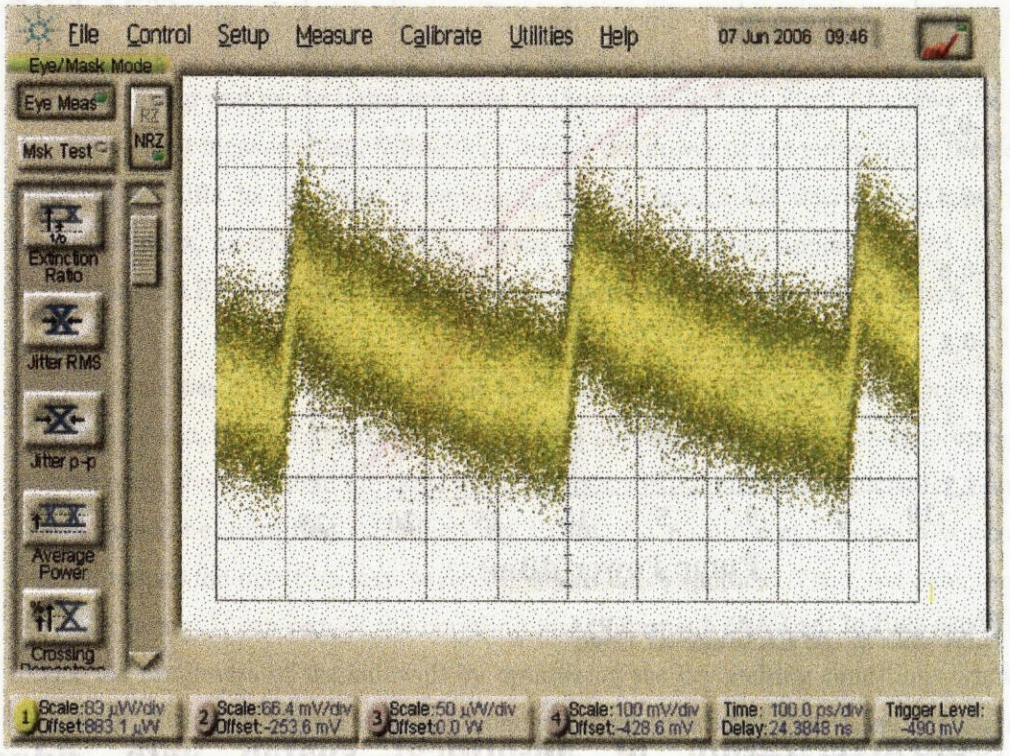

Fig.5.16 Waveform of the output of the after the switch from 1540nm to 1550nm.

In order to find out the reason, we investigated the performance of the EAM and MMI.

5.6.2 Loss measurement

According to the design, the total length of the device is 3.5mm. We measured the passive waveguide with InGaAsP (Q1.25) and obtained the loss, 18dB/cm. Similar to (5.1)
EAM: 51.8dB/cm

$$\begin{cases} 150\times\alpha_{EAM} + 2c + 200\times\alpha_{waveguide} = 1.497 \\ 100\times\alpha_{EAM} + 2c + 250\times\alpha_{waveguide} = 1.328 \end{cases} \tag{5.2}$$

So the coupling loss between the active EAM and passive waveguide can be obtained by solving the above equations. c= 0.18dB, which means 95.9% coupling efficiency. This result is consistent with those in subsection 5.5.1.

The measured insertion loss is 30dB. It is consisted of 2*6dB/facet coupling loss between tapered fibers and device, 1dB EAM propagation loss together with the coupling loss at the

interface of the active EAM and passive waveguide, 3*3 dB MMI loss and 8dB loss of the passive waveguide whose core layer is composed of InGaAsP (Q1.25).

5.6.3 XPM of EAM

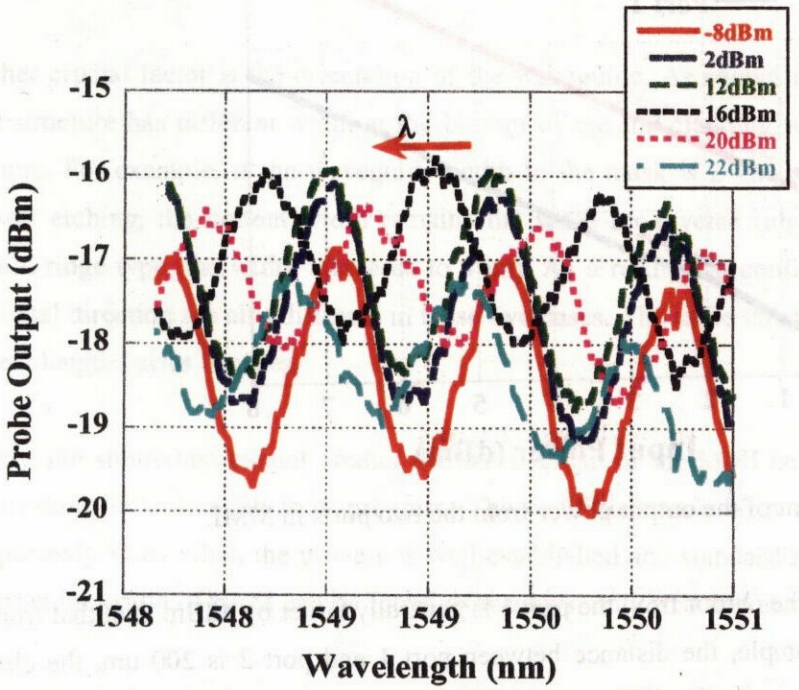

Fig.5.17 Fabry-Perot measurement for XPM of the EAM with ridge waveguide.

From Fig.5.17, strong XPM has been observed, and when the input power is 22dBm, the phase shift is more than 2π. These results confirm that the EAM works well as the phase modulator in the all-optical switch.

5.6.4 Characterization of MMI

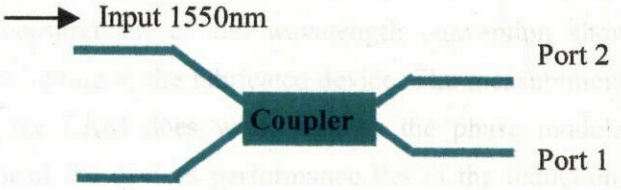

Fig.5.18 Schematic view of the MMI.

Both the input and output are coupled to the tapered fibers. The input light is set in TE mode.

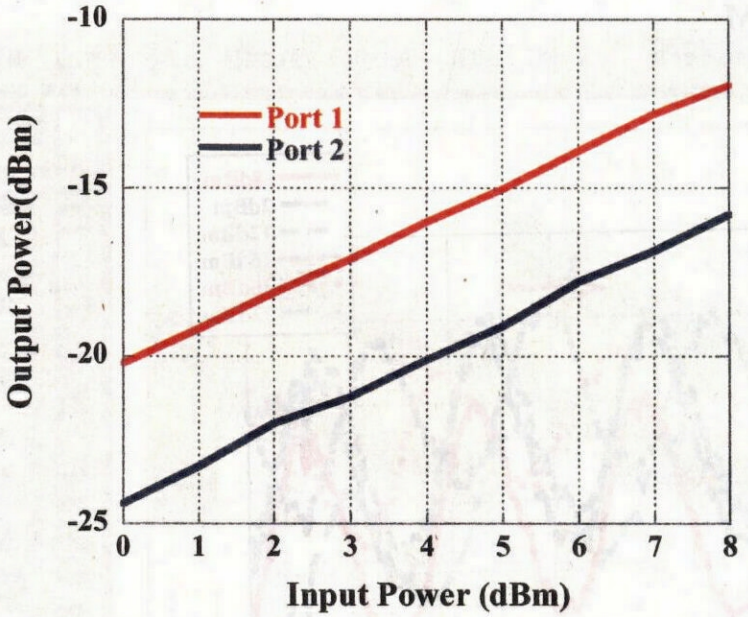

Fig.5.19 Measurement of the output power from the two ports in MMI.

Fig.5.19 shows that the output from the port 1 is generally larger by 4dBm than that from port 2. Because in the sample, the distance between port 1 and port 2 is 200 um, the cleavage conditions are the same, so the difference of the power is due to the MMI. Notice that in the all-optical switch, there are three MMIs in series, and they will cause totally 12dB unbalance possibly.

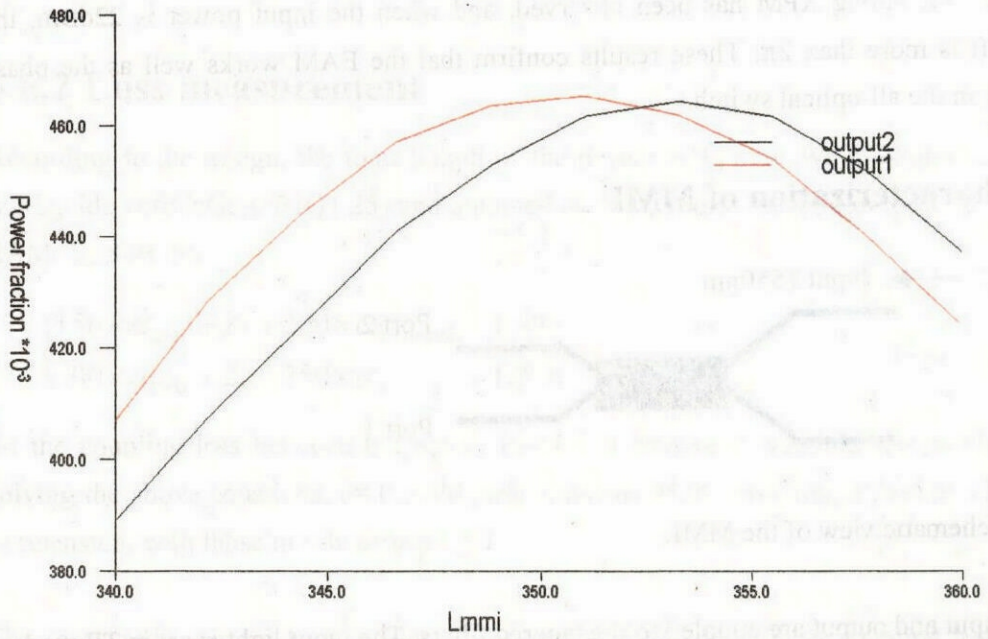

Fig.5.20 Ratios of output power at two ports as function of the MMI length.

Actually, taking the tolerance in the process into account, we make three EAMs varying from 340um to 360 um. Due to the damage in the process, only the device with 340um EAM was measured. The change of the length may be the main reason for the unbalance of the MMI. Fig.5.20 shows the simulation result of the balance between two outputs of the MMI. We can see that the balance is sensitive to the change of the length. The larger the length difference with 355um, the larger the difference of the outputs.

Another crucial factor is the orientation of the waveguide. As shown in Fig.3.7, the reverse ridge structure has different width at the bottom of the InP cladding with the forward ridge structure. For example, if the waveguide width in the mask is 2 um, after photolithography and wet etching, the bottom width remains the same for reverse ridge waveguide, but for forward ridge type, the width increases to 4 um. As a result, the confinement factors in the horizontal direction are also different in these two cases. The same thing happens to MMI and the beat length varies in cases.

Frankly, the simulation cannot predict the exact length of the MMI because in my case, the optimization of fabrication is in progress. The conditions vary with time and errors occur unexpectedly. Only when the process is well established and standardized in my experiment, the optimum length of EAM can be found. Nowadays, only trial and error can help.

5.7 Summary

In this chapter, we proposed a novel all-optical switch by using two EAMs on the arms in the MZ interferometer. The switch is fabricated on the substrate grown by two-step regrowth technique described in Chapter II. We optimized the fabrication process of the devices in both ridge and high mesa cases. Then both of these two devices were carefully measured. In the all-optical waveguide with high mesa, because the insertion loss is so large due to the sidewall roughness and doping in the passive region, no dynamic operation was carried out. However, the static measurement of the wavelength conversion shows primary evidence for the all-optical switching of the fabricated device. The measurement of the XPM in a single EAM shows that the EAM does work well as the phase modulator by XPM. Therefore, the improvement of the devices performance lies in the reduction of the insertion loss. For this purpose, then an all-optical switch with ridge structure was fabricated. The measurement of the loss in the whole device shows that the loss can be reduced by 20 dB even when the total length is longer than the high mesa structure. The dynamic wavelength conversion of 2.5Gb/s has been measured. Though the converted signal is of very poor quality, it is an evidence for the availability of the all-optical switches. Further investigation was done on MMI and EAM

by cutting them from the whole switch. Experiments showed that in the EAM, XPM was clearly observed. This means the poor converted signal does not come from the EAM. On the other hand, the measurement of the output power in a single MMI showed 4dB unbalance between two output ports, which meant maximum 12dB unbalance in the whole device. We believe this is the main reason for the small extinction ratio in the dynamic wavelength conversion. By optimizing the MMI, dynamic performance of the all-optical switch can be improved.

References

[1] Foo Cheong Yit, Xueliang Song, Haizheng Song, Zhenrui Zhang, Masakazu Sugiyama, and Yoshiaki Nakano, "Dynamic Switching and Wavelength Conversion in a Monolithically Integrated Michelson-Interferometric SOA All-Optical Switch by Selective Area MOVPE", IPRM '05, Glasgow, May8-12, 2005.

[2] Xuelin Yang, R.J. Manning, R.P. Webb, R. Giller, F. Gunning, D. Cotter, "High-speed All-optical Signal Processing using Semiconductor Optical Amplifiers", International Conference on Transparent Optical Networks, Vol(2), pp.161 – 164, 2006

[3] S. Nakamura, K. Tajima, "Bit-rate-transparent nonreturn-to-zero all-optical wavelength conversion at up to 42 Gb/s by operating symmetric-Mach-Zehnder switch with new scheme", OFC 2004 Vol(2), pp.23-27, 2004

[4] Foo Cheong Yit, Xueliang Song, Haizheng Song, Zhenrui Zhang, Masakazu Sugiyama, and Yoshiaki Nakano, "Demultiplexing Operation in a Monolithically Integrated Michelson Interferometer SOA All-Optical Switch by Single-Step Selective Area MOVPE", ECIO '05, Oral session, Grenoble, Apr6-8, 2005.

[5] S. Nakamura, T. Tamanuki, Y. Ueno, K. Tajima, "Ultrafast optical demultiplexing, regeneration, and wavelength-conversion with symmetric-Mach-Zehnder all-optical switches" OFC 2003,Vol.1, pp.346 – 347, 2003

[6] M. Eiselt, "Optical Loop Mirror with Semiconductor Optical Amplifier", Electron. Lett., vol. 28, no.16, pp. 1505-1507, July 1992.

[7] N.E. Dahdah, R. Coquille, B. Charbonnier, E. Pincemin, C. Kazmierski, J. Decobert, A. Vedadi, G. Aubin, A. Ramdane, "All-optical wavelength conversion by EAM with shifted bandpass filter for high bit-rate networks", Photonics Technology Letters, Vol.18(1), pp.61-63, 2006

[8] Zhaoyang Hu, Hsu-Feng Chou, K. Nishimura, M. Usami, J.E. Bowers, D.J. Blumenthal,; "Optical clock recovery circuits using traveling-wave electroabsorption modulator-based ring oscillators for 3R regeneration", Selected Topics in Quantum Electronics, Vol.11(2), pp.329 – 337, 2005

[9] H. Murai, M. Kagawa, H. Tsuji, K. Fujii, "80-Gb/s Error-Free Transmission Over 5600 km Using a Cross Absorption Modulation Based Optical 3R Regenerator", Photonics Technology Letters, Vol.17(9), pp.1965 – 1967, 2005

[10] "Characterisation of a MQW electroabsorption modulator as an all-optical demultiplexer", L.K. Oxenlowe, F. Romstad, A. Tersigni, S. Hojfeldt, K. Yvind, P.M.W. Skovgaard, K. Hoppe, J. Hanberg, LEOS 2001, Vol.1(12-13), pp.36 – 37, 2001

[11] E.J.M. Verdurmen, Y. Liu, G.D. Khoe, H. de Waardt, , "Study on the limits of all-optical time-domain demultiplexing using cross-absorption modulation in an electroabsorption modulator" Optoelectronics, Vol.153(2), pp.75 – 83, 2006

[12] K. Nishimura, R. Inohara, M. Tsurusawa, M. Usami, "Delayed-Interferometric Wavelength Converter Using Electroabsorption Modulator with Optimized Bandgap Wavelength", ECOC 2002. Vol.1(08-12), pp.1 – 2, 2002

[13] M. Kato and Y. Nakano, "Wavelength conversion using polarization dependence of photo-induced refractive index change in an MQW-EA modulator," Tech. Digest IPR '2001, IMG5, (2001)